

Electrochemical Society Proceedings volume
STATE OF THE ART APPLICATION OF SURFACE AND INTERFACE ANALYSIS METHODS TO
ENVIRONMENTAL MATERIAL INTERACTIONS
D.R. Baer, C.R. Clayton, G.P. Halada, G.D. Davis, Editors

**CHARACTERIZATION OF SALT PARTICLE-INDUCED CORROSION
PROCESSES BY SYNCHROTRON-GENERATED X-RAY FLUORESCENCE
AND COMPLEMENTARY SURFACE ANALYSIS TOOLS**

Aaron K. Neufeld¹, Ivan S. Cole¹, Alan M. Bond², Hugh S. Isaacs³
and Scott A. Furman¹

¹ CSIRO Building, Construction and Engineering
PO Box 56, Highett, Victoria 3190, Australia

² School of Chemistry, Monash University
PO Box 23, Clayton, Victoria 3800, Australia

³ Department of Applied Science, Brookhaven National Laboratory
Upton, New York 11973, USA

ABSTRACT

The benefits of using synchrotron-generated X-rays and X-ray fluorescence analysis in combination with other surface analysis techniques have been demonstrated. In studies of salt-induced corrosion, for example, the detection of Rb ions in the area of secondary spreading when salt-containing micro-droplets are placed on zinc surfaces, further supports a mechanism involving cation transport during the corrosion and spreading of corrosive salt on exposed metal surfaces. Specifically, the new analytical data shows that: (a) cations are transported radially from a primary drop formed from a salt deposit in a thin film of secondary spreading around the drop; (b) subsequently, micro-pools are formed in the area of secondary spreading, and it is likely that cations transported within the thin film accumulate in these micro-pools until the area is dehydrated; (c) the mechanism of cation transport into the area of secondary spreading does not include transport of the anions; and (d) hydroxide is the counter ion formed from oxygen reduction at the metal surface within the spreading layer. Data relevant to iron corrosion is also presented and the distinct differences relative to the zinc situation are discussed.

INTRODUCTION

With recent advances in computerized technology and analysis techniques, the study of chemical reactions that occur on surfaces can now be “visualized” as they occur in real time. This ability offers the corrosion scientist a unique opportunity to study the

mechanistic details of processes which have theoretically been attributed in the past to degradation science. In particular, the domains that are now accessible include the interface between the metal surface and its micro-climate. The micro-climate has been defined as the environment which a metal surface experiences, when the physical domain of the micro-climate is of the order of millimetres. Of particular interest in the interface region are processes like electrochemical reactions, diffusion, precipitation and adsorption, and the formation of unique surface species.

In the modern era, the key to obtaining detailed information about a particular system is the use of a wide range of analytical techniques that give complementary information. For example, Neufeld *et al.* (1, 2) have elucidated many aspects of the mechanism of corrosion initiation when a salt particle is wetted on the surface of zinc by using a combination of data obtained from X-ray microprobe, infra-red microscope and scanning Kelvin probe techniques. In these studies, it was deduced that the corrosion processes that result when sodium chloride particles are wetted on zinc metal, cations and anions are transported within the thin layers of electrolyte that form as a result of secondary spreading, (2) and that ions are transported specifically because of the electrochemical reactions that are occurring at the metal surface. Cations are transported to regions of cathodic activity, and anions are transported to regions of anodic activity. The conclusions imply that the transport of ions is likely to be the most important factor in a corrosion process, as it will determine the magnitude and rate of the dissolution reactions. Consequently, monitoring and measuring the rate of ion transport for a corrosion process should enable advantageous modification of corrosion protection systems (oxides, surfactants, barrier coatings) so that they become much more effective in blocking corrosion initiation reactions.

In this report, the database on the subject has been expanded by the employment of in-situ synchrotron studies which significantly extend knowledge concerning the transport of ions. The synthesis of information from this and previously used techniques is also discussed with respect to atmospheric corrosion processes. Importantly, new results presented in this paper show that by performing the initiation experiment and monitoring the distribution of ions spatially and temporally, using synchrotron X-ray light, detailed determination of ion transport behavior is possible, so that fundamental issues related to the transport of ions for the mechanism of initiation can be more fully understood.

EXPERIMENTAL

Zinc and iron (99.9%, Goodfellow) surfaces having a mirror finish were prepared by firstly grinding with 800 SiC and then with 1200 SiC paper in water, and then progressively polishing with 9, 3 and 1 micron diamond pastes on Struers cloths. The surfaces were rinsed with ethanol and dried with inert gas. Initiation experiments were performed using either micro-crystals of sodium chloride or micro-droplets of 1M NaCl solution. Procedures for conducting the corrosion initiation experiments have been described elsewhere. (2) For the synchrotron studies, solutions of sodium chloride (1.0M) containing rubidium and bromide (0.05M) were prepared using analytical-grade reagents. Rubidium and bromide were added for detection purposes, because sodium and chloride excitation energies are below the energy window set by the beamline monochromator associated with the elemental detection by the X-ray fluorescence method. It was found that the ratio of sodium to rubidium used allowed both the natural chemistry resulting

from the chloride-induced corrosion to develop, and at the same time the concentrations of rubidium and bromine were high enough to be detected by X-ray fluorescence. Solutions of sodium and rubidium were used instead of solid salt particles to ensure that the required element ratios were reproducibly achieved in the initiation experiments. Some solutions used to make micro-droplets also contained corrosion inhibitor species such as $\text{Cr}_2\text{O}_7^{-2}$, WO_4^{-2} and MnO_4^{-2} in a concentration range of 10^{-4} to 10^{-2} M. Using a micro-syringe, a droplet of approximately 0.02 microliters was placed on the surface of the metal. Specimens were rapidly mounted in a perspex chamber which was covered with a 6 micron thick mylar film that also acted as the X-ray window. The humidity in the chamber was controlled using a bubbler system which sparged air through distilled water. Typical airflow rates were about 1 L min^{-1} . The nature of the compressed air was important because of the critical role of carbonate salt formation, and hence the experiments were conducted using bottled medical-grade air, which retains the required small amounts of CO_2 . The perspex chamber was mounted on the stepper motor-driven translation stages and the micro-droplet was examined with a video microscope. The focal point of the microscope was also the focus point of the X-ray beam. The experimental set-up is illustrated in Figure 1. By moving the translation stage, scans over the area of corrosion and spreading could be obtained. The X-ray beam spot size was determined by reference to a razor edge to be approximately 25 microns in diameter and oval in shape, due to the incident angle of 45° on the sample. During linescans, steps of between 25 and 50 microns were used, and X-rays counted for between 2 and 4 seconds (depending on the beam current). Element intensities were corrected for variations in beam intensity.

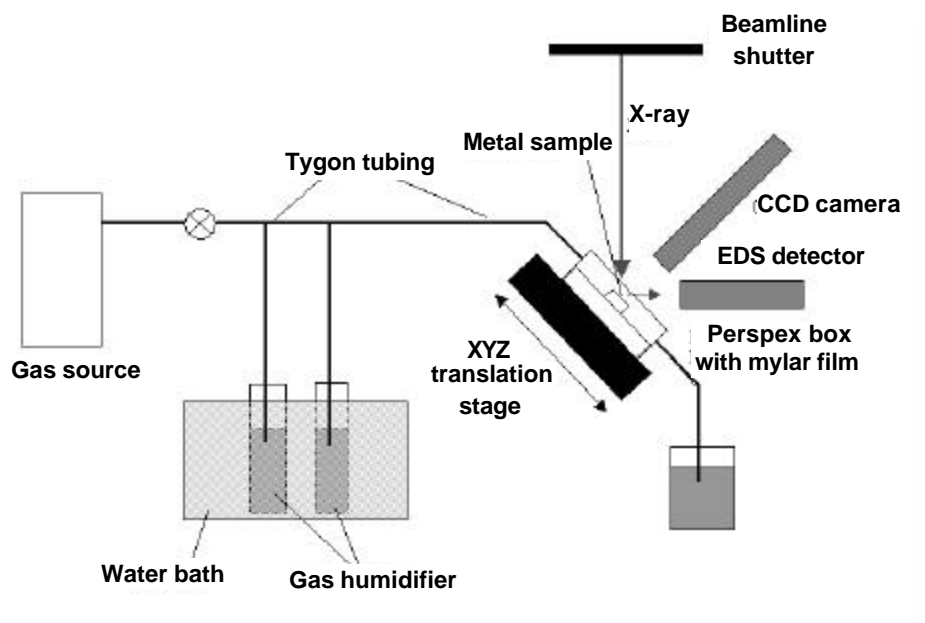


Figure 1: Experimental set-up used for synchrotron X-ray fluorescence studies.

RESULTS AND DISCUSSION

Description of the initiation process

Although visible to the naked eye, the physical development of the corrosion process was best observed with the aid of a video microscope system. Figure 2 presents two images from different stages of the spreading process on zinc. After approximately

10 minutes from the placement of the salt droplet, a thin film commences to radiate outward symmetrically from the hemispherical droplet, as shown on the left-hand side of Figure 2. Shown on the right-hand side is the droplet and a thin film which is clearly present after approximately 35 minutes, and which is associated with the so-called “secondary spreading” process. (2) During the course of the secondary spreading process, corrosion products become visible in the center of the droplet. The secondary spreading process was not affected by the vertical position of the sample or by the pulsing of the stepping motors. During most of the secondary spreading process, the aspect of the droplet edge to the surface of the metal is maintained, as illustrated in Figure 3.

After 120 minutes, the volume of the droplet becomes significantly reduced, and solid compounds are observed at the perimeter of the thin film. After 7 hours, the initiation area is completely dehydrated, and at the center of the affected area there are dark grey corrosion products surrounded by a white ring. The boundary, or perimeter, where the secondary spreading has ceased is also white in colour. From previous studies, (2) the dark grey corrosion products are zinc hydroxychloride and the white rings are composed of sodium carbonate. Chloride is only detected in the central region where the droplet was placed, and sodium is only detected in the rings of carbonate compounds formed at the perimeter of the original droplet and at the perimeter of the region resulting from secondary spreading.

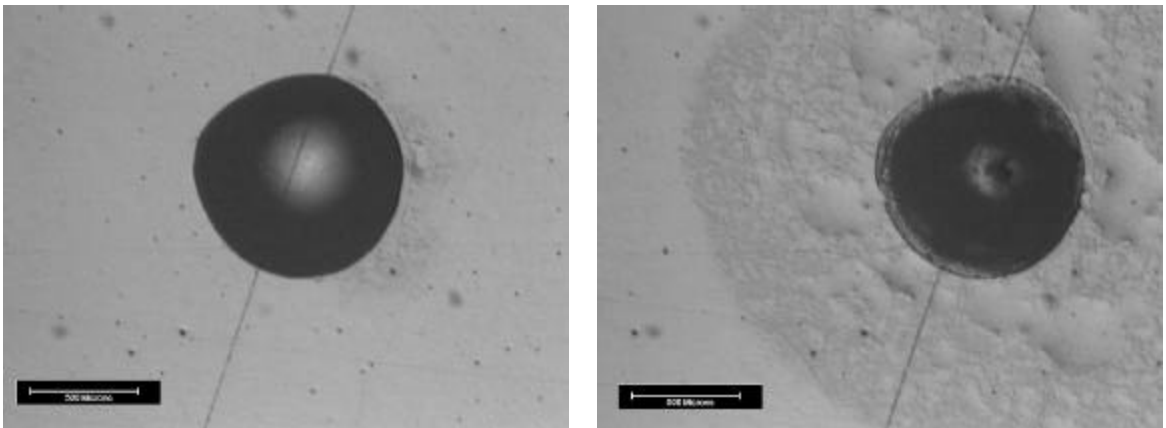


Figure 2: Micro-droplet and secondary spreading during a typical corrosion initiation experiment on zinc. Droplet immediately after placement (left) and after 20–30 minutes (right).

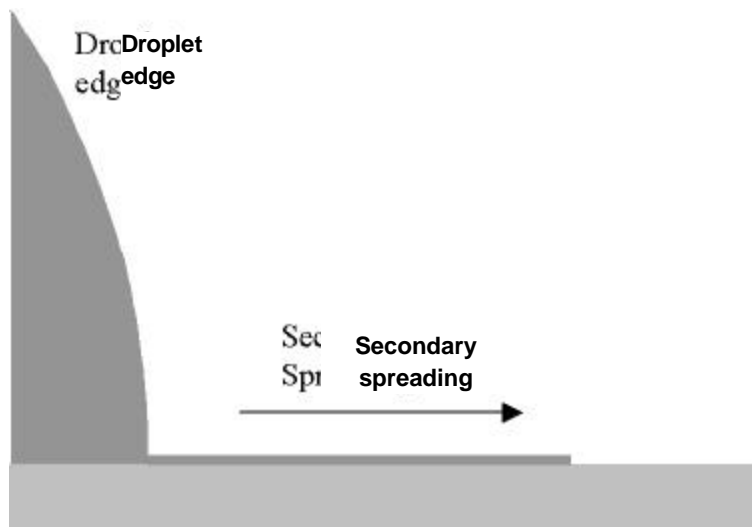


Figure 3: Diagrammatic representation of secondary spreading at the droplet edge. The basic geometry of the droplet is maintained despite the propagation of the thin film which is associated with the secondary spreading process.

Transport of ions during the initiation of corrosion on zinc

The transport of ions is believed to be responsible for the propagation of the thin layer in secondary spreading on zinc. If the postulate that the area resulting from secondary spreading is the site of cathodic reactions is correct, i.e. oxygen reduction, then Rb ions should be transported along with the Na ions to this region. Linescans were performed starting from the center of the droplet to a point radially just outside the expected final perimeter of the secondary spreading area. Figure 4 shows the corrected intensity of Rb as a function of time and position which represents the Rb ion concentration in the droplet and the surrounding thin film. This data illustrates important aspects concerning the transport of Rb as the corrosion process proceeds. At the start of the experiment, the center of the droplet is located at 2.0 mm, and the edge at about 1.8 mm. It can be seen that secondary spreading has progressed from the droplet edge at 1.8 mm to about 1.1 mm – a distance of about 0.5 mm. For the first 50 minutes, the film spreads very quickly, but the highest concentration of the Rb remains within the micro-droplet.

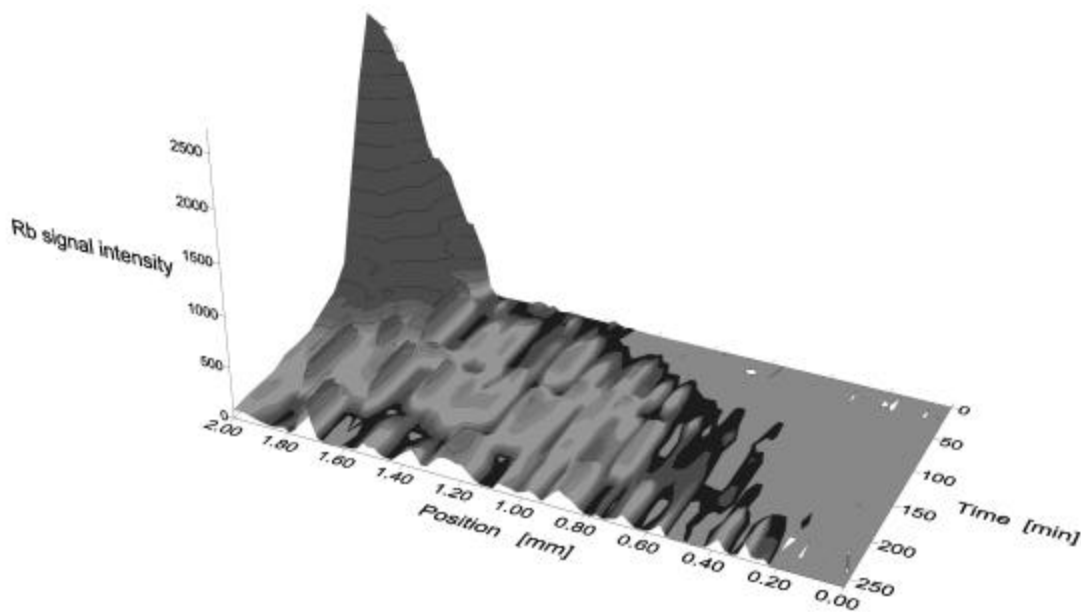


Figure 4: Rubidium intensity with respect to time and position on the zinc surface from about 10 to 260 minutes.

After 60 minutes, the signal intensity of Rb in Figure 4 is becoming much greater in the area surrounding the droplet, whereas the signal intensity of Rb within the droplet area decreases significantly. This is consistent with Rb ions being transported from the droplet into the thin film.

Transport of ions and electroneutrality

Ions of positive and negative charge cannot be separated over a distance of the order of hundreds of microns. Essentially positive and negative ions must accompany each other when they are transported from one region to another. The above microprobe studies showed that Rb is transported to the same region where Na was previously found. Based on theoretical considerations, Neufeld *et al.* (2) argued that cations can be transported to the area of spreading, whilst maintaining electroneutrality, and without transport of chloride because oxygen reduction at the metal surface in this area generates hydroxide, a counter ion for cations. Therefore, in the present case, the anions (namely Cl and Br) can be held in the region of anodic activity where metal is being oxidized to metal ions. However, prior to this in-situ study, the mechanism of ion transport could only be inferred on the basis of ex-situ measurements and could not be absolutely known. One of the goals of this X-ray study was to directly measure the behavior of anions during the secondary spreading process, and hence the Br concentration was monitored in addition to Rb. Shown in Figure 5 is the ratio of Rb to Br during a linescan after 6 hours at high humidity (>90%). The droplet is in the region from 2000–2400 microns, where the ratio is extremely low due to the transport of Rb ions to the secondary spreading region. The secondary spreading perimeter is around 1200 microns, so that this region to about 2000 microns is the secondary spreading region where very high Rb:Br ratios are found. Thus, it is very clear that Br is not being transported with the cations Na or Rb during the initiation process. This result is also consistent with the hypothesis that the initiation process is driven by electrochemical reactions that are intrinsically linked, so that distinct transport of cations occurs.

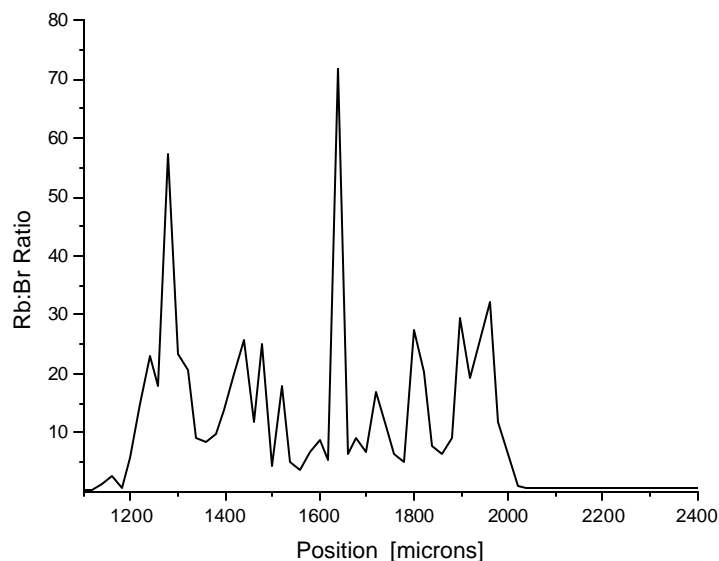


Figure 5: Ratio of Rb and Br concentrations after 6 hours in humid conditions.

The original droplet is located in the region greater than 2050 microns. Transport of Rb from the droplet into the area of secondary spreading has occurred without the transport of Br as predicted theoretically in earlier studies. (2)

Changes in the area of secondary spreading during time

In the present study, some attention was also given to the region of secondary spreading and the nature of the thin electrolyte film as a function of time. Figure 6 presents an optical image of the secondary spreading area near the edge of the thin film region, represented as a contour map of Rb signal intensity over that area. It appears that micro-pools have formed within the thin film. It is deduced from analysis of the images in Figure 6 that the “nodes” detected in the linescan measurements of the secondary spreading area are actually micro-pools of solution containing Rb ions. However, analysis of linescans as a function of time show that arrays of very small micro-pools slowly become more concentrated with Rb ions and then merge to form a larger micro-pool. These micro-pools are very unlikely to be physically moving across the surface of the metal, so it is assumed that Rb ions are being transported through the thin film to the micro-pools as a result of the secondary spreading process.

Secondary spreading on iron

Corrosion studies were also performed on iron in the same manner as on zinc, and although some features differed, generally the same transport processes take place during secondary spreading. The corrosion behavior of a droplet of salt solution has been documented by Evans. (3) Since the iron surface at the edge of the droplet would also be the site of cathodic behavior, it is reasonable to postulate that secondary spreading would proceed as observed with zinc. No reports on this phenomenon occurring with iron have been found, possibly because the spreading may have represented only a small fraction of the drop size, and hence it would be difficult to detect by conventional analysis techniques.

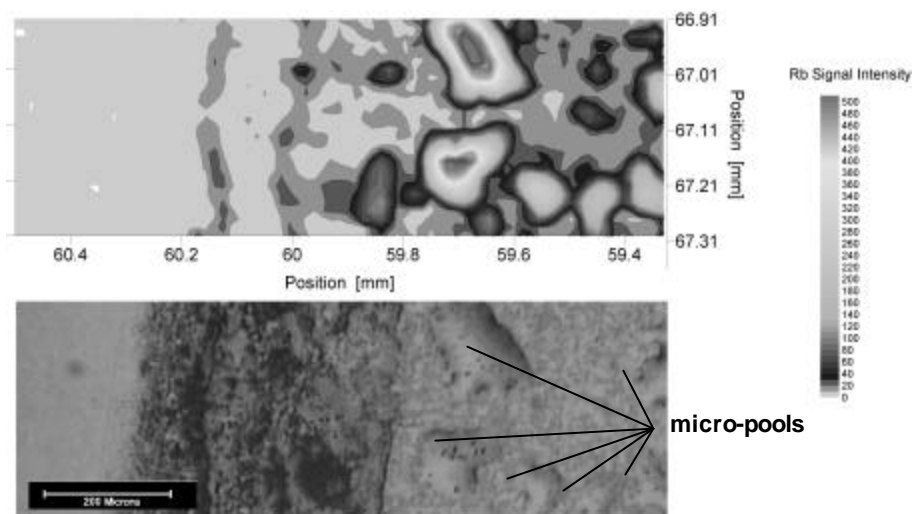


Figure 6: Image of the secondary spreading area near the perimeter (bottom) and a contour map of the Rb intensity of that area (top). The formation of micro-pools explains the “nodes” of high Rb signal intensity observed in the linescans (see Figure 5).

Shown in the top section of Figure 7 are images captured 15 minutes and 4 hours after the placement of a micro-droplet onto the iron surface. In this case, while secondary spreading is not visible, the detection of micro-pools is at least consistent with observations from the initiation experiment on zinc. In fact, the formation of micro-droplets on iron appears to correspond with surface scratches from the polishing process. To confirm that the formation of these micro-pools is associated with a secondary spreading process and not simply with the nucleation and condensation of water, Rb:Br elemental analysis was performed over the area of the surface where micro-pools had formed. As was also observed in experiments with zinc metal, a high ratio is detected within the micro-pools (see lower part of Figure 7), which is consistent with transport of Rb not being accompanied by transport of Br.

The absence of visible secondary spreading on iron made it more difficult to define a boundary, than is the case with zinc. With zinc it appeared that the surface was wetted and micro-pools developed on the wetted surface. On iron, this wetted surface was apparently absent, but the micro-pools still developed. Two separate processes may be considered to be taking place: one a wetting process that is not visible, and the other a nucleation process forming micro-pools. In contrast, on zinc, many small micro-pools form producing a visible spreading. On iron only a few micro-pool nucleation sites form. However, these must be fed by a wetted surface as Rb is observed to migrate across the surface to the larger micro-pools. Analysis of time-lapse video microscope recordings during this process are planned for future experiments, and should significantly assist in understanding the nuances of the iron system.

The effect of inhibitors on the secondary spreading process

The effect of an inhibitor on the secondary spreading process has been studied. Since the secondary spreading process is also initiated by localized anodic activity, the addition of an inhibitor should prevent the spreading process. The selection of inhibitors studied included $\text{Cr}_2\text{O}_7^{-2}$, WO_4^{-2} and MnO_4^{-2} , although only the effects of WO_4^{-2} on iron could be

analyzed using X-ray fluorescence because unfortunately the Zn K_{α} and the W L_{α} emission lines overlap, and the lower energy of the Cr and Mn emissions were swamped out by the background scattering from the metal substrates. Thus, only the Fe, W combination could be studied directly, although on zinc the processes which resulted in visible changes were studied using the video microscope and analysis of Rb and Br.

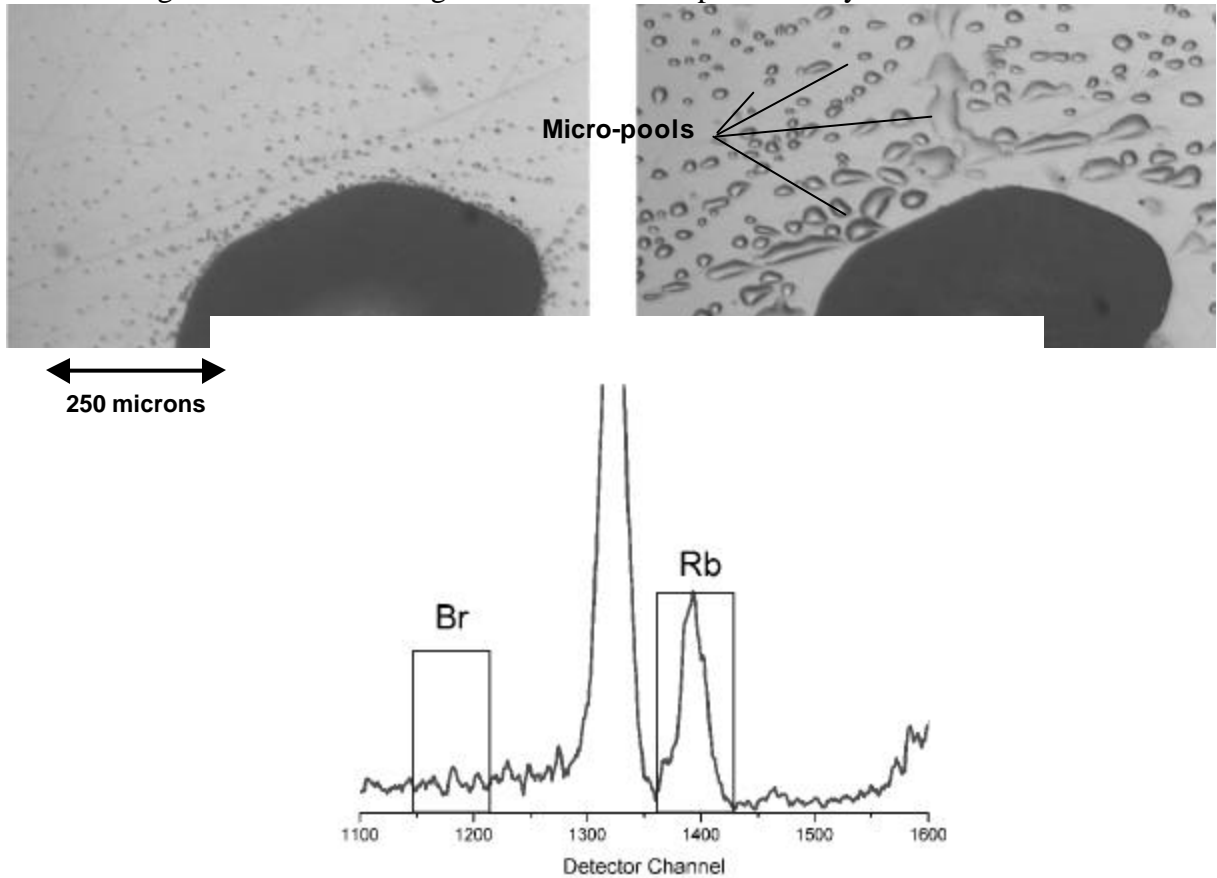


Figure 7: Images at 15 minutes (top left) and 4 hours (top right) after commencement of the corrosion initiation experiment on iron with a salt micro-droplet. The formation of micro-pools is consistent with observations from the analogous initiation experiment on zinc. Shown below is the X-ray spectrum acquired from a micro-pool after 4 hours. The rectangles indicate the regions of the Br K_{α} and Rb K_{α} line energies and the dominance of Rb in comparison with Br, as also detected using zinc metal.

Additions of dichromate on zinc resulted in two types of corrosion behavior. At concentrations of 10^{-4} and 10^{-3} M in 1M NaCl, secondary spreading initially progressed faster than observed without dichromate. However, the final diameter reached was only half the distance found without the dichromate. Without the addition of dichromate, corrosion products appeared to precipitate evenly across the surface of the zinc and no localized corrosion precipitates formed within the droplet. With low concentrations of dichromate, localized corrosion products were observed at the center of the micro-droplet that grew as the secondary spreading process took place. With the addition of 10^{-2} M dichromate, no corrosion products nor thin film as a result of secondary spreading were observed. The addition of WO_4^{-2} or MnO_4^{-2} concentrations up to 10^{-2} M to the halide solutions resulted in similar behavior to that of low concentrations of dichromate on zinc, where secondary spreading and localized corrosion products formed. Plausibly, these oxyanions are not effective cathodic inhibitors, and hence oxygen reduction is allowed to proceed.

The effects of the oxyanions $\text{Cr}_2\text{O}_7^{-2}$ and WO_4^{-2} on iron were investigated. Experiments conducted with 0.01M concentrations of inhibitor showed that secondary spreading had occurred in the sense that, as in previous iron investigations, high Rb:Br ratios were detected within the micro-pools. Importantly, in experiments with WO_4^{-2} present, W could be detected in addition to the Rb and Br ions. That is, W had accumulated within the droplet either as a hydrated tungsten oxide or as an insoluble iron tungstate. The location of the precipitate is illustrated in Figure 8. On the right-hand side is an image of the corrosion products near the center of the hemispherical droplet, and on the left-hand side is a contour map of the W intensity for the corresponding area.

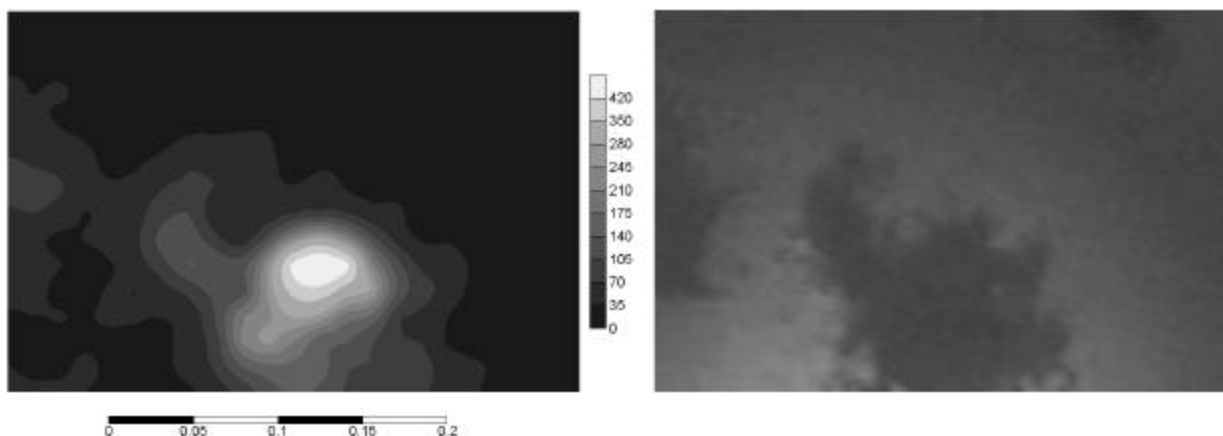


Figure 8: Visual image of corrosion products formed on the surface of iron (under the hemispherical droplet) (left) and the corresponding intensity contour map for W in this area (right). The scale bar beneath the intensity map indicates the size in mm.

CONCLUSIONS

The benefits of using synchrotron-generated X-rays and X-ray fluorescence analysis in combination with other surface analysis techniques have been demonstrated. The detection of Rb ions in the area of secondary spreading when salt micro-droplets are placed on zinc surfaces further confirms the proposed mechanism involving cation transport during the corrosion and spreading of corrosive salt deposits on exposed metal surfaces. Specifically, the new analytical data has shown that during salt-induced corrosion:

- For many hours cations are transported radially from a primary drop formed from a salt deposit in a thin film of secondary spreading around the drop.
- Micro-pools are formed in the area of secondary spreading, and it is likely that cations transported within the thin film accumulate in these micro-pools until the area is dehydrated.
- The mechanism of cation transport into the area of secondary spreading does not include transport of anions. The ratio of Rb to Br in the secondary spreading area indicates that hydroxide is the counter ion formed from oxygen reduction at the metal surface within the spreading layer.

ACKNOWLEDGEMENTS

The authors would like to thank CSIRO and ANSTO for support in meeting travel costs from Australia to the Brookhaven National Laboratory. Our appreciation is also extended to T. Lanzorotti and B. Rao who kindly assisted in operating the beamline X26A at the National Synchrotron Light Source, Brookhaven National Laboratory. The work was carried out, in part, under the auspices of Department of Energy, Division of Materials Sciences, Office of Science under contract No. DE-AC02-98CH10886.,

REFERENCES

1. Neufeld, A. K.; Cole, I. S.; Bond, A. M.; in *Scanning Probe Microscopy for Electrode Characterisation and Nanometer Scale Modification*, Hansen, D., Isaacs, H., The Electrochemical Society Proceedings Series, Pennington, NJ (2001).
2. Neufeld, A. K.; Cole, I. S.; Bond, A. M.; Furman, S. A.; *Corrosion Science* (in press).
3. Evans, U. R.; *Corrosion and Oxidation of Metals*, Arnolds, London (1960).